On the effect of substrate viscoelasticity on the evaporation kinetics and deposition patterns of nano-suspension drops

Yuhong Chen[1], Alexandros Askounis[2], Vasileios Koutsos[3],

*Prashant Valluri[1], Yasuyuki Takata[4,5], Stephen K. Wilson[6], and Khellil Sefiane[1]**

1 Institute for Multiscale Thermofluids, School of Engineering, University of Edinburgh, The King's Buildings, Mayfield Road, Edinburgh, EH9 3JL, United Kingdom

2 Engineering, Faculty of Science, University of East Anglia, Norwich Research Park, Norwich, NR4 7TJ, United Kingdom

3 Institute for Materials and Processes, School of Engineering, University of Edinburgh, The King's Buildings, Robert Stevenson Road, Edinburgh, EH9 3FB, United Kingdom

4 International Institute for Carbon-Neutral Energy Research (WPI-I2CNER), Kyushu University, 744 Motooka, Nishi-ku, Fukuoka 819-0395, Japan

5 Department of Mechanical Engineering, Thermofluid Physics Laboratory, Kyushu University, 744 Motooka, Nishi-ku, Fukuoka 819-0395, Japan

6 Department of Mathematics and Statistics, University of Strathclyde, Livingstone Tower,

26 Richmond Street, Glasgow, G1 1XH, United Kingdom

KEYWORDS: drop evaporation, viscoelastic substrate, nanofluids, particle deposition

ABSTRACT: This study investigates the evaporation of sessile pure water and nano-suspension drops on viscoelastic polydimethylsiloxane (PDMS) films. We varied the viscoelasticity of the PDMS films by controlling the curing ratio, and categorized them into three types: stiff (10:1, 20:1, 40:1), soft (60:1, 80:1), and very soft (100:1, 120:1, 140:1, 160:1). On stiff surfaces, pure water drops initially evaporate in a constant contact radius (CCR) mode, followed by a constant contact angle (CCA) mode, and finally in a mixed mode of evaporation. Nano-suspension drops follow the same trend as water drops but with a difference towards the end of their lifetimes, when a short second CCR mode is observed. Complete evaporation of nano-suspension drops on stiff substrates leads to particle deposition patterns similar to a coffee ring with cracks and deposition tails. On soft surfaces, the initial spreading is followed by a pseudo-CCR mode. Complete evaporation of nano-suspension drops on soft substrates leads to deposits in the form of a uniform ring with a sharp ox-horn profile. Unexpectedly, the initial spreading is followed by a mixed mode on very soft substrates, on which wetting ridges pulled up by the vertical component of surface tension are clearly observed in the vicinity of the contact line. As the evaporation proceeds, the decreasing contact angle breaks the force balance in the horizontal direction at the contact line and gives rise to a net horizontal force, which causes the contact line to recede, transferring the horizontal force to the wetting ridge. Due to the viscoelastic nature of the very soft substrate, this horizontal force acting on the wetting ridge cannot be completely

countered by the bulk of the substrate underneath. As a result, the wetting ridge moves horizontally in a viscous-flow way, which also enables the contact line to be continuously anchored to the ridge and to recede relative to the bulk of the substrate. Consequently, a mixed mode of evaporation occurs. Complete evaporation of nano-suspension drops on very soft substrates leads to finger-like deposits.

INTRODUCTION

The evaporation kinetics of and the deposit formation from sessile suspension drops on rigid substrates have been widely investigated due to their widespread industrial applications such as those in film coating, nanotechnology and biomedicine. However, deformable substrates are also of considerable interest as they occur in many practical situations, such as biological sample analysis using lab-on-a-chip technology[1], microfluidic devices[2], and thermoregulation of the human body[3]. In particular, drop evaporation on soft substrates provides a promising low-cost method for the fabrication of three-dimensional structures at the microscale using capillary origami[4].

To illustrate the evaporation kinetics of drops on soft substrates, let us first briefly summarize those on rigid substrates. A sessile drop of pure liquid will evaporate in one of three evaporation modes, namely a constant contact radius (CCR) mode, a constant contact angle (CCA) mode, or a mixed mode[5], the latter involving a variety of different stick-slip behaviours of the contact line[6-9]. In colloidal drops the evaporation kinetics are accompanied by complex internal and interfacial flows, leading to a variety of deposition patterns being formed after complete evaporation. Examples include coffee rings, multiple concentric rings, uniform coverage deposits, and even complicated finger-like patterns[10-18].

A soft substrate cannot balance the vertical component of surface tension at the contact line of the drop without deforming, and so a wetting ridge is pulled up at the contact line. Such surface deformation enables Neumann's law rather than Young's law to govern the force balance at the contact line[19,20]. Using transmission X-ray microscopy, Park *et al*.[21] observed the bent cusps of static wetting ridges whose tips are capable of a small rotation on a viscoelastic silicone gel. These authors also developed a dual-scale (*i.e.* microscopic and macroscopic) approach to analyse the asymmetric geometry of the ridges. In addition, they distinguished three different mechanisms, specifically, "viscoelastic-braking", "stick-slipping" and "stick-breaking" behaviours, which characterise the propagation of the ridges[22]. They pointed out that contact line pinning is weakened by spontaneous spreading of a moderately developed ridge, but enhanced by cusp bending of a fully developed ridge during the sticking stage of the motion. Moreover, Kajiya *et al*.[23] proposed the viscous flow of the ridge as another mechanism of drop spreading, and demonstrated that which mechanism dominates depends on the advancing velocity of the contact line.

Apart from the wetting ridge at the contact line of the drop, a dimple underneath the drop induced by capillary pressure was experimentally confirmed by the observation of fluorescent drops on flexible PDMS substrates by Rusanov[24]. However, this study was limited to treating the viscoelastic layers as semi-infinite bodies and hence neglected the influence of the underlying stiff glass substrates. By changing the thickness of viscoelastic film, Pericet-Camara *et al*.[25] showed that the underlying substrate has an influence on the depth of the dimple when the deformation exceeds 8% of the thickness of the soft layer. Furthermore, the profile of the soft layer has troughs on either side of the ridge. In addition, the theoretical and numerical results of

Yu and Zhao[26] indicate that there exists a limiting membrane thickness of the order of a millimetre below which the thickness of a flexible membrane influences surface deformation.

However, the sessile drops described above did not evaporate significantly due to either the non-volatile nature of the liquid or the saturated vapor environment. For evaporating drops, Pu and Severtson[27] observed that a water drop on a highly viscoelastic acrylic polymer surface first spreads and then undergoes a CCR mode. In contrast, on a stiff PDMS substrate the drop undergoes a multistep evaporation process comprising CCR, CCA and mixed modes in sequence. The different evaporation kinetics indicate that the larger wetting ridge formed on softer substrates promotes the pinning of the contact line, and thus extends the duration of the CCR mode. A similar conclusion was drawn by Yu *et al*.[28] and Lopes and Bonaccurso[3] for the evaporation of water drops on PDMS substrates with different viscoelasticities. The soft substrates shorten the lifetimes of the drops due to a longer CCR mode, which results in a larger evaporation rate than in a CCA mode[5].

In addition, Lopes and Bonaccurso[29] added silica microspheres to a water drop in order to investigate the effect of substrate viscoelasticity on the evaporation-induced particle deposition patterns. In contrast to a pure water droplet, the contact line re-pins after the CCA mode and a second CCR mode occurs during the final stage of evaporation. They found that on softer substrates, although a longer CCR mode occurs, the particles deposit into a less pronounced coffee ring, indicated by a smaller ratio of deposit heights measured at the centre and the rim of the coffee ring. This differs from the behaviour on rigid substrates, where the CCR mode enhances the formation of a coffee ring due to the occurrence of radially outward capillary flow transporting particles to the contact line region[10,30]. Instead, Lopes and Bonaccurso[29] demonstrated that the receding contact line also enables particles to accumulate at the contact

line, and thus to form a coffee ring. Furthermore, some deposits, whose height depended on the velocity of the receding contact line, were left behind during the CCA mode.

From the brief review provided above, it is evident that, although the influence of substrate viscoelasticity on the evaporation of drops of pure liquids has been investigated, there has to date been only limited work on drops of suspensions and on the resulting particle deposition patterns. Moreover, the viscoelastic substrates described in the literature, both gel and PDMS, were all limited to relatively stiff cases, as characterised by Young's moduli of the order of kPa or MPa in magnitude[3,27-29]. One may therefore ask, what happens if the Young's modulus of the substrate is reduced by several orders to Pa? In particular, does the horizontal (rather than the vertical) displacement of the soft substrate affect the evaporation kinetics of the drop? Is the motion of contact line relevant to the motion of the wetting ridge? In order to address these questions, in the present study we produced PDMS substrates with a broad range of viscoelasticity with shear moduli ranging from kPa to several Pa. We firstly carried out experiments on the evaporation of pure water drops to understand the fundamental phenomena, and then we conducted a further series of experiments with the sessile aqueous SiO_2 suspension drops. The morphologies of the deformed substrates after complete evaporation were imaged in order to understand the interaction between the soft substrates and the drops. The deposition patterns of particles left behind on the substrates, which were found to be strong functions of both the evaporation kinetics and the surface deformation, were also observed.

MATERIALS AND METHODS

PDMS solutions with various viscoelasticities were made by varying the volume ratio of monomer to curing agent (Sylgard 184, Dow Corning Corporation, USA). To be specific, nine curing ratios, namely 10:1, 20:1, 40:1, 60:1, 80:1, 100:1, 120:1, 140:1 and 160:1, were prepared

as follows: (1) mix the monomer and curing agent at the required curing ratio and stir the blend manually with a stainless steel rod; (2) thoroughly mix and degas the mixture in a centrifuge (Low Speed Centrifuge LC-100, Tomy, Japan) at varying speeds from 1000 rpm to 2000 rpm.

Soft films were fabricated as follows: (1) sonicate a glass slide of thickness 1 mm in a bath of ethanol (99.5%, Wako Pure Chemical Industries Ltd., Japan) for 10 minutes at 20℃, then rinse with deionized water and dry under a stream of compressed air; (2) spin coat (Mikasa spincoater 1H-DX2, Japan) PDMS blends on the cleaned glass slides at 1000 rpm for 60 s; (3) dry the substrate in an oven (DV400, Yamato, Japan) at 80℃ for 2 hours. The PDMS films were 75±5 µm thick and their roughness, indicated by Ra, are 0.005, 0.005, 0.004, 0.005, 0.003, 0.002, 0.003, 0.002 and 0.002 µm as the curing ratio increases from 10:1 to 160:1. Both of these parameters were measured using a 3D laser scanning confocal microscope (LSCM) (OLS4000 LEXT, Japan).

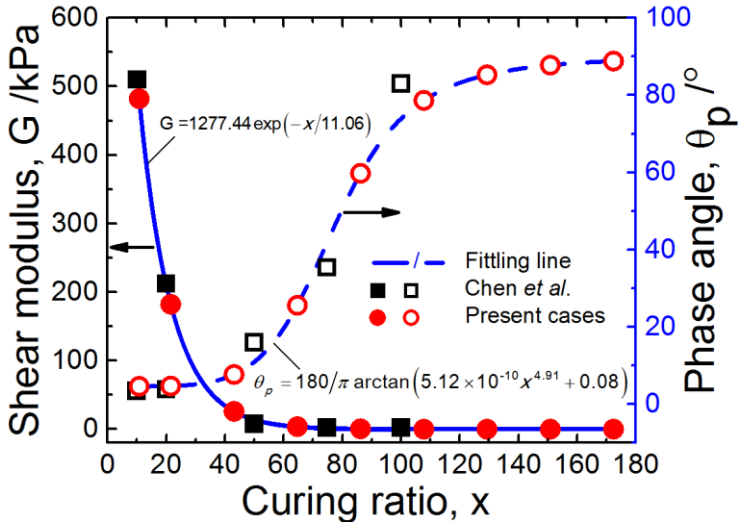

Figure 1. Shear modulus and phase angle of PDMS samples at 1 Hz reproduced with permission from Chen *et al.*[31] and the estimated values for the present PDMS samples.

In Fig. 1 we fitted the data for the shear modulus and phase angle of PDMS measured by Chen *et al.*[31] with an exponential function, $G = 1277.44\exp(-x/11.06)$, and an arctangent function, $\theta_p = (180/\pi)\arctan(5.12\times10^{-10}x^{4.91}+0.08)$, respectively, where G, θ_p and x denote the shear modulus, phase angle and curing ratio by mass, with correlation coefficients of 0.99976 and 0.96563, respectively. Then we used the fitted functions to estimate the shear moduli and phase angles of our PDMS samples (red solid and open circles in Fig. 1) so that their viscoelasticity is quantified. The phase angle here relates the loss and storage moduli, which is 0° for pure elastic and 90° for pure viscous materials. As shown in Fig. 1, the softness and viscosity of PDMS increase with the curing ratio. PDMS is hard and mostly elastic for curing ratio 10:1, but very soft and mostly viscous for curing ratio 160:1.

A water-based solution of 0.125 wt% SiO_2 nanoparticles of diameter 80 nm was used as the nano-suspension. Different concentrations are obtained by diluting the concentrated solution (Klebosol, AZ Electronic Materials France SAS, Trosly-Breuil, France). To ensure the homogenous dispersion of particles, the solution was placed in a sealed bottle and sonicated for 30 s prior to each experiment. Meanwhile, pure deionized water drops were used as control experiments.

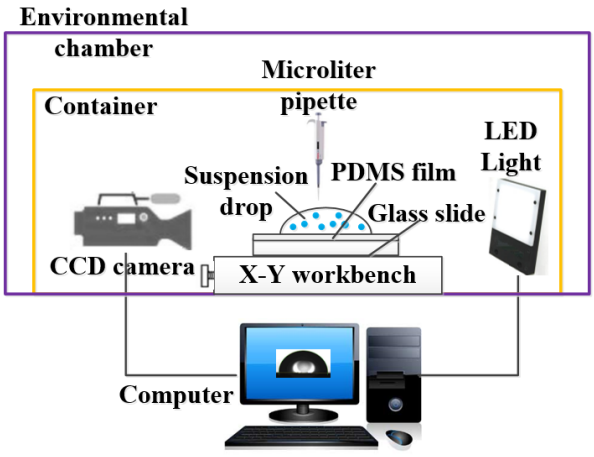

Figure 2. A schematic diagram of the experimental setup.

The experimental setup, illustrated in Fig. 2, consisted of an environmental chamber (PR-3KT, ESPEC Corp., Japan) to control the relative humidity at 51±5% and temperature at 21±0.5℃. A CCD camera (STC-TB152USB-AS, SENTECH, Japan) and an LED back light were positioned at the opposite sides of the XY-axis workbench to image the drop profile at the centre of the chamber at 4.815 frames per second. The soft substrate was placed on a XY-axis workbench and a drop of approximately 3 μl was generated by a pipette and gently deposited on to it. Then a 45 cm × 33 cm × 35 cm container was used to cover the drops in order to minimize disturbances due to ambient convection. The container was roughly about 100 times bigger than the drop. The real-time video of the profile of the drying drop was processed using ImageJ® and MATLAB® software. Then the evolutions of the drop wetting angle and the contact diameter in time were extracted using the assumption of a spherical cap. After each complete evaporation, the deformed morphologies of the soft substrates and the particle deposits were imaged by both compact stereo microscope (ZEISS Stemi 305, Carl Zeiss Microscopy, USA) and LSCM. The latter also provides the profiles of the deposition patterns. In what follows, we will present representative examples of our results.

RESULTS AND DISCUSSION

In this section, details of the evaporation of pure water drops as well as the associated surface deformations are presented for each of the different viscoelastic substrates. We then address the influence of the substrate softness on the evaporation kinetics of water-SiO_2 suspension drops, which is compared to that of pure water drops in order to elucidate the effect of the nanoparticles. Finally, the various deposition patterns on each substrate are described.

Evaporation kinetics of pure water drops. We first performed control experiments to demonstrate how the evaporation of pure water drops proceeds on deformable substrates, as shown in Fig. 3.

On the stiffest substrate (*i.e.* the one of curing ratio 10:1), the evaporation starts with a CCR mode until about 315 s (marked with a red dashed line), which is followed by a CCA mode until about 1765 s (marked with a magenta dashed line), and finally by a mixed mode until the complete evaporation. This sequence is in agreement with the previous observation of Pu and Severtson[27]. With increasing substrate softness, the duration of the CCR mode is extended from 315 s on the 10:1 substrate to 1550 s on the 20:1 substrate and 1780 s on the 40:1 substrate, respectively. Additionally, the CCA mode disappears in the latter two cases.

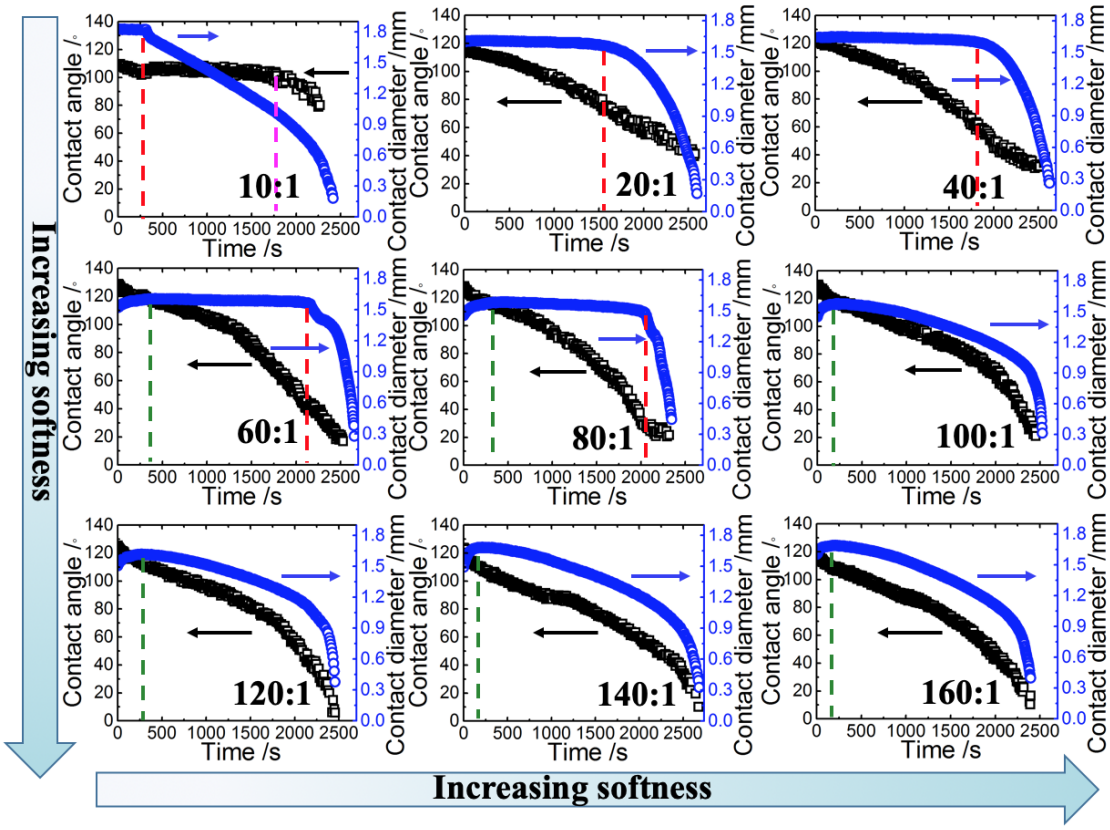

Figure 3. Evolution of contact angle and contact diameter over time of pure water drops evaporating on the different viscoelastic substrates. Red, magenta and green dashed lines mark the end of (pseudo-) CCR mode, the CCA mode, and the spreading, respectively.

On soft substrates (*i.e.* for curing ratios of 60:1 and 80:1), the drops spread during the initial stage of evaporation (marked with a green dashed line). As discussed by Shanahan[32] and Carré and Shanahan[33], the spreading of a drop on a soft substrate is dominated by the excess capillary energy, which is mainly consumed by the substrate viscoelastic dissipation during surface deformation, whereas by the viscous dissipation in the drop on a hard substrate. The former mechanism slows down the initial advance of the contact line so that its spreading is easily captured in the video. Subsequent to the spreading, the contact line seems to pin there, but, in reality, it actually recedes very slowly. Such a behaviour of the contact line is not strictly a CCR mode and is therefore called a pseudo-CCR mode, which lasts for about 1800 s on the 60:1 substrate and 1700 s on the 80:1 substrate. The duration of the CCR mode accounts for 13%, 60%, 67%, 68% and 72% of the drop lifetime as the curing ratio increases from 10:1 to 80:1, respectively. This gradual increase in the duration of the CCR mode with the substrate softness suggests that greater surface deformation occurs at the contact line, which gives rise to a greater energy barrier for contact line motion.

On very soft substrates (*i.e.* for curing ratios of 100:1, 120:1, 140:1 and 160:1), the contact line initially advances before retracting. The durations of the initial advancing stage are about 205 s, 250 s, 180 s and 170 s, respectively, for the curing ratios mentioned above. However, on soft substrates this initial advancing stage is of an extended duration (340 s for 60:1 and 330 s for 80:1). After spreading, the contact line recedes on very soft substrates, leading to the mixed mode of evaporation. This behaviour occurs only on very soft substrates and, to the best of our

knowledge, is reported for the first time here. This behaviour is particularly unexpected given the similar roughness of all the substrates (which affects the contact angle hysteresis and hence the pinning behaviour[6,34]). According to our results for stiff and soft substrates, and those reported in references[27,28,35], the contact line should have been prevented from retreating by the prominent wetting ridge formed on these very soft substrates. However, the fact is that the contact line recedes not only in the evaporation of pure water drops but also in that of nano-suspension drops, where the presence of particles is capable of strengthening the pinning behaviour[28]. We will analyse this seemingly paradoxical result in a later section.

Surface deformation after complete evaporation of pure water drops. As discussed above, the evaporation kinetics of drops as well as the behavior of the contact line depends strongly on the wetting ridge formed on soft substrates, whose height is proportional to the ratio of the vertical component of surface tension to the shear modulus of the substrate[36]. We imaged the substrates prior to drop deposition, immediately after drop drying, 10 hours after drop drying, and several days later, as shown in Fig. 4, in order to gain insight into the different surface deformations of the substrates after complete evaporation.

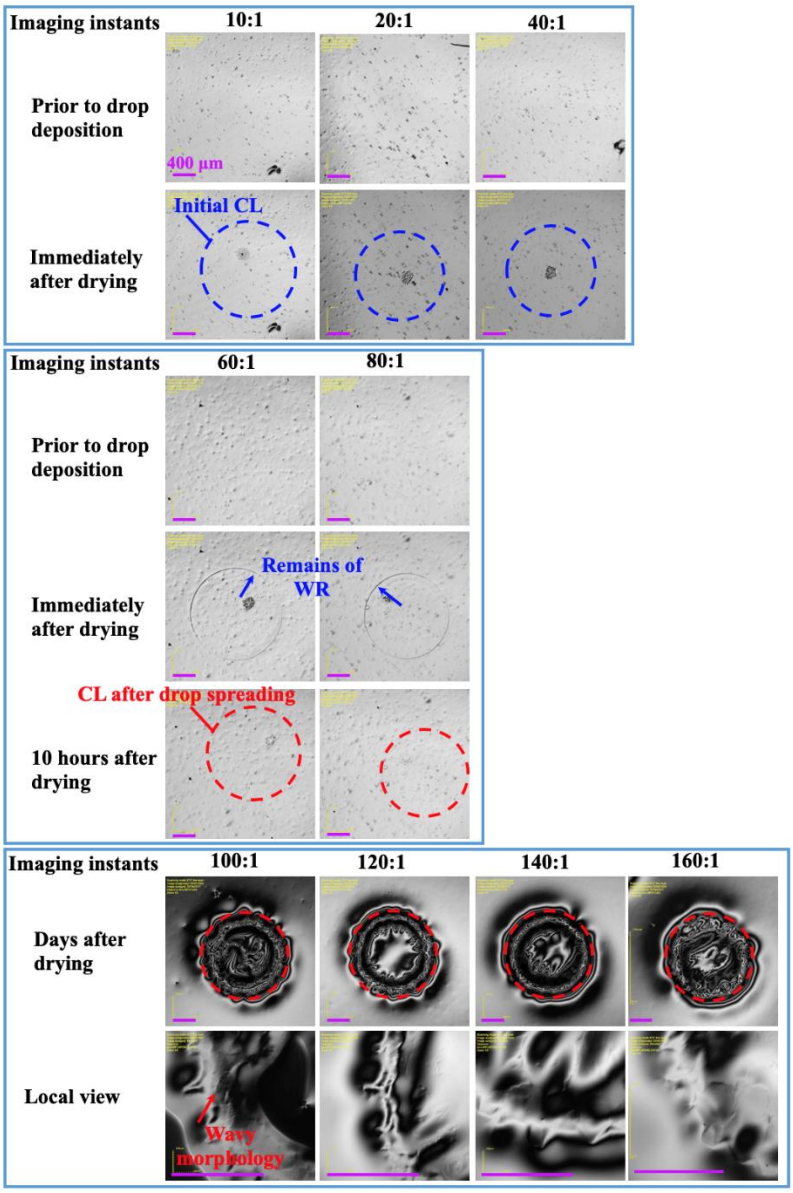

Figure 4. Surface deformations of the different viscoelastic substrates imaged at different instants: prior to drop deposition (for a reference), immediately after drop drying, 10 hours after drop drying, and several days later. The blue and red dashed lines mark the position of the initial contact line (CL) on stiff substrates and the farthest position of the contact line after drop spreading on soft and very soft substrates, respectively. The blue arrows point to the remains of wetting ridge (WR) on soft substrates, which are located at the farthest positions of the contact line. The magenta scale bars in all of the images are 400 μm.

On stiff substrates (10:1, 20:1, 40:1), no trace of the wetting ridge is apparent after complete evaporation due to the fact that surface deformation recovers elastically and instantaneously as soon as the surface tension force disappears. In contrast, the wetting ridge on soft substrates (60:1, 80:1) is clearly visible after the drop evaporates, and is roughly located at the farthest position of the contact line due to the drop spreading. Nevertheless, the wetting ridge gradually disappears and the substrate recovers in approximately 10 hours. Such a response of strain to stress corresponds to a high elastic deformation of the viscoelastic material. On the other hand, very soft substrates (100:1–160:1) exhibit permanent deformations, which remain even several days after drop evaporation. Essentially, very soft substrates deform plastically, similarly to the unrecoverable deformation of stretched chewing gum. Using a higher magnification microscope, details of the wavy morphologies of the deformed substrates are shown in the bottom images in Fig. 4, labelled “Local view”.

The differing deformation relaxations of these substrates are determined by the two characteristic aspects of viscoelastic materials, namely their elastic and viscous properties. The former is responsible for the elastic (reversible) deformation while the latter is responsible for the plastic (irreversible) deformation. We have observed three different deformation regimes: elastic deformation of stiff substrates, mixed (viscoelastic) deformation of soft substrates, and plastic deformation of very soft substrates, which clearly indicate that with increasing curing ratio, the viscous component of the viscoelastic substrates increases whereas the elastic component decreases.

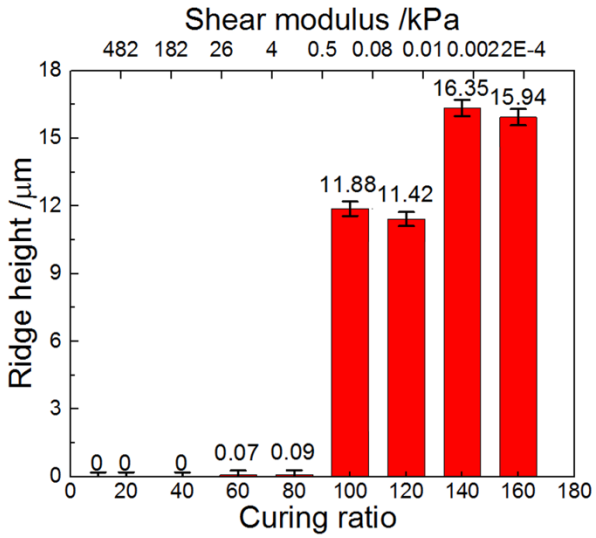

Figure 5. The height of the wetting ridge after complete evaporation plotted as a function of the curing ratio and the shear modulus of the substrate.

Fig. 5 shows the height of the wetting ridge after complete evaporation, plotted as a function of the curing ratio and the shear modulus of the substrate. On stiffer substrates (10:1–40:1), the wetting ridge quickly recovers after drop evaporation due to the elastic deformation. Hence, we regard the ridge height in these cases as zero. As the substrate softness increases, the substrate cannot fully balance the surface tension force without deforming, resulting to small deformations on soft substrates of approximately 0.07 μm (60:1) and 0.09 μm (80:1), and more pronounced plastic deformations for very soft substrates of approximately 11.88 μm (100:1), 11.42 μm (120:1), 16.35 μm (140:1), and 15.94 μm (160:1). Our observations agree well with previous work by Shanahan and Carré[36] in which the height of the wetting ridge was found to be inversely proportional to the shear modulus of the substrate.

Evaporation kinetics of nano-suspension drops. Let us now turn our attention to nano-suspension drops. As shown in Fig. 6, on the stiffest substrate (10:1), the drop initially evaporates in a CCR mode followed by a CCA mode, and then a mixed mode. Increasing substrate softness lengthens the CCR mode from 350 s on the 10:1 substrate to 1080 s and 1280 s

on the 20:1 and 40:1 substrates, respectively, and shortens the CCA mode from 1150 s on the 10:1 substrate to 300 s on the 20:1 substrate, while it disappears entirely on the 40:1 substrate. This behaviour is similar to that of pure water drops on the same substrates, *i.e.* stiff ones. On soft substrates (60:1 and 80:1), the drops spread initially, followed by a pseudo-CCR mode of approximately 1650 s and 1700 s on the 60:1 and 80:1 substrates, respectively. The duration of the CCR mode accounts for approximately 15%, 44%, 58%, 76% and 78% of the lifetime of the drops on the substrates mentioned above. Indeed, excluding the initial spreading on the soft substrates, the CCR mode can constitute as much as 92% and 93% of the lifetime of the drop. This finding further supports our previous claim that the softness of the substrates enhances the pinning of the contact line and hence the CCR mode. On the other hand, the drops on the very soft substrates (100:1–160:1) undergo a mixed mode after initial spreading.

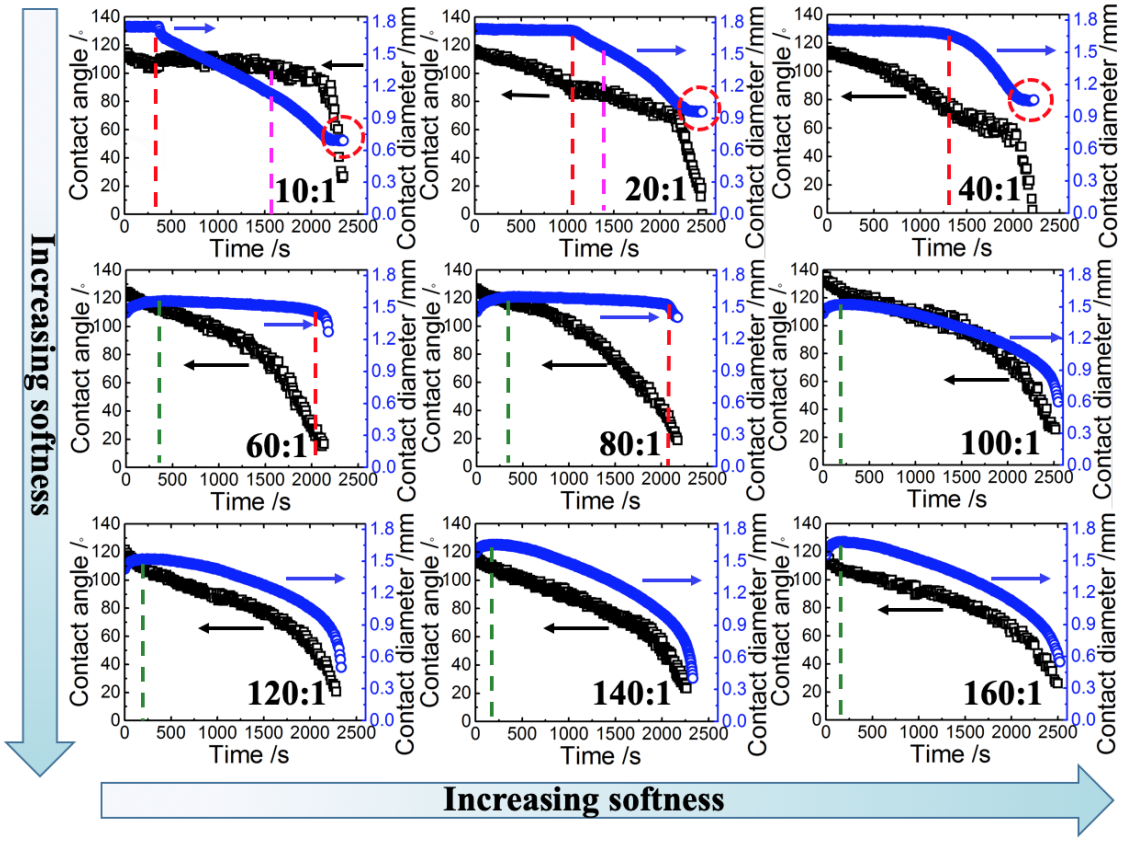

Figure 6. Evolution of contact angle and contact diameter over time of nano-suspension drops evaporating on different viscoelastic substrates. Red circles mark the second CCR mode on the stiffer substrates. Red, magenta and green dashed lines mark the end of the CCR mode, the CCA mode, and the initial spreading, respectively.

The addition of nanoparticles results in re-pining of the contact line near the end of the evaporation on stiff substrates due to particle deposition impeding contact line motion[6]. Additionally, the duration of the CCR mode for nano-suspension drops (15%, 44%, 58%, 76% and 78%) on stiff and soft surfaces (10:1, 20:1, 40:1, 60:1 and 80:1) are compared with those of pure water drops (13%, 60%, 67%, 68% and 72%), respectively. This comparison indicates that generally, the CCR mode lasts longer for nano-suspension drops due to the enhancement of contact line pinning by the particles. The 20:1 and 40:1 substrates on which the CCR mode is shorter are outliers, probably arising from the preferential pinning of one side of the contact line on these substrates. The second CCR mode observed for stiff substrates may influence the final deposition pattern, which we discuss in a later section.

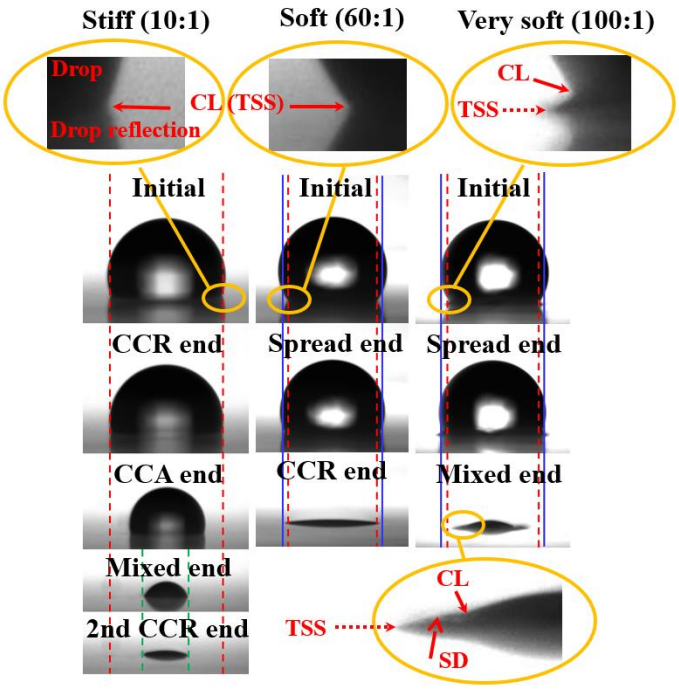

Figure 7. Representative images of the evaporation of nano-suspension drops on different viscoelastic substrates. The red and green dashed lines mark the initial contact dimeter and the contact diameter in the second CCR mode, respectively, and the blue solid line marks the maximum contact diameter. The ellipses show zooms of the contact line, and the arrows point at the contact line (CL), the top surface of the substrate (TSS), and the surface deformation (SD), respectively.

Wetting ridge and contact line motion dynamics. Fig. 7 shows representative images of the evaporation of nano-suspension drops on each type of substrate. The initial contact diameter and the contact diameter in the second CCR mode are marked by the red and green dashed lines, respectively, and the maximum contact diameter by the blue solid line. In the top left and top centre images, the contact line (CL) of the drop and the top surface of the substrate (TSS) are aligned on stiff and soft substrates and the wetting ridge is too small to be captured by the CCD camera. On the other hand, in the top right image, the wetting ridge extending from the CL to the

TSS on very soft substrates is readily apparent. Similar wetting ridges occur for drops on lubricant-impregnated textured surfaces[37,38]. More significantly, we observe that a highly irregular and broad wetting ridge, like a bump, is formed inside the original wetted area for the very soft substrates. This is very different from the highly regular ring-like deformation which occurs for the other substrates.

Inspired by the motion of the wetting ridges on the very soft substrates, we relate the unexpected mixed mode observed here to the dynamics of the wetting ridge. Fig. 8 illustrates two regimes of wetting ridge dynamics (denoted as Regimes 1 and 2) which occur in succession when an evaporating drop recedes on a very soft substrate.

In Regime 1, the decrease in the contact angle as the drop evaporates leads to an increase in the surface tension force in the horizontal direction, encouraging the contact line to depin. The contact line attempting to depin transmits a horizontal force to the wetting ridge. Due to its viscoelastic nature, the very soft substrate behaves like a viscous liquid and cannot counter this horizontal force. Hence, the ridge moves in a viscous-flow way (*i.e.* creep deformation[22,39]), as shown in Fig. 8. The ridge moves from its old position (denoted by a red dot) to its new position (denoted by a red star). The ridge is large enough to tightly anchor the contact line, preventing it from depinning, and so the ridge and the CL the move together. This results in the observed mixed mode, with simultaneous decrease in the contact angle and the contact diameter shown in Fig. 6. This is similar to the continuous slip of an advancing drop on a gel substrate when the viscous-flow regime dominates[23].

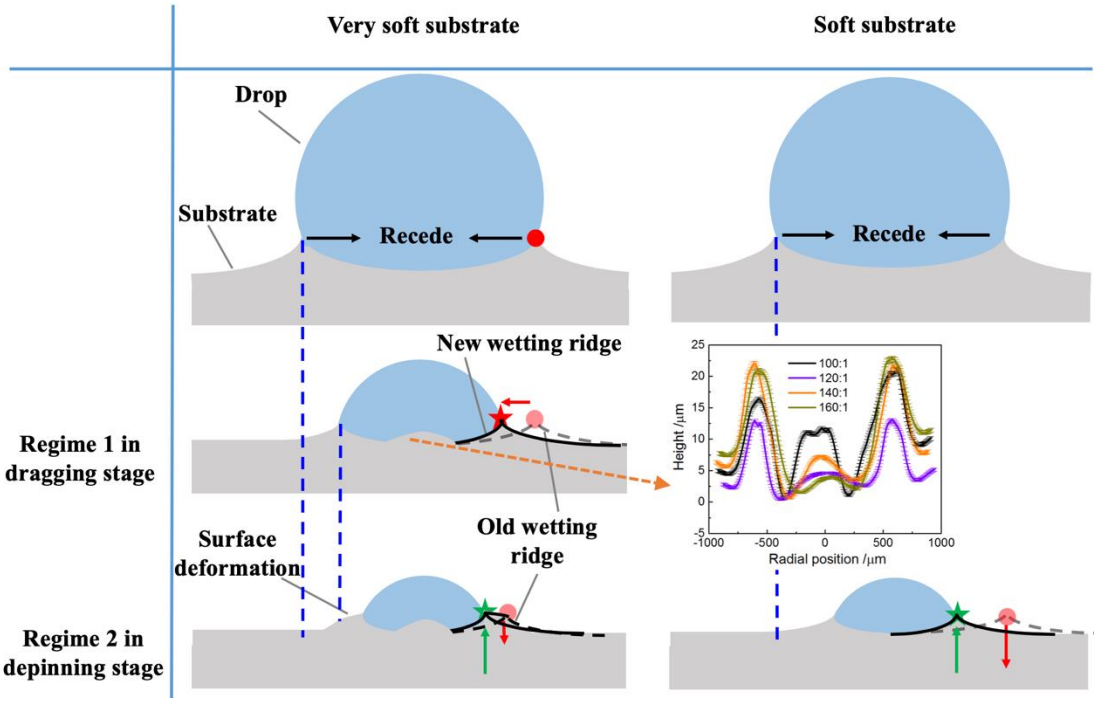

Figure 8. Schematic illustration of the regimes of wetting ridge dynamics when the contact line recedes on viscoelastic substrates. Regime 1: The ridge moves from its old position (denoted by a red dot) to its new position (denoted by a red star) with the contact line. Regime 2: The retraction of the drop is faster than the substrate can cope with, leading to contact line slipping. The new ridge grows (shown by the green star and arrow), while the height of the old ridge decreases (shown by the red dot and arrow), but the old ridge (shown by the black dashed line) cannot fully recover its original shape due to the plastic deformation. The inset shows the height profiles of the surface deformation on very soft substrates. The soft substrates are harder to move horizontally than the very soft ones, and when the drop re-pins the old ridge fully recovers (shown by the red dot and arrow) as the new ridge grows (shown by the green star and arrow).

This behaviour of the contact line is qualitatively different from the usual pinning or depinning behaviour, and the anchoring of the contact line to the wetting ridge means that, in spite of the plastic deformation, the retraction of the drop does not to leave a wetting ridge behind at its old

position. This is clearly demonstrated by the bump-like surface deformation occurring inside, rather than at, the maximum diameter of the contact line in our experiments, as shown in Fig. 7. Furthermore, the horizontal motion of the wetting ridge compresses the substrate under the drop, generating a local peak in the surface deformation rather than the smooth dimple previously reported in the literature[25]. The inset in Fig. 8 shows the height profiles of the surface deformation on the very soft substrates after the evaporation of a water drop which clearly demonstrate this behaviour.

In Regime 2, the retraction of the drop is faster than the substrate can cope with, leading to contact line slipping[22,23]. We ascribe the bump-like surface deformation to the combined effects of the plastic deformation of the very soft substrate (shown in Fig. 4) and Regime 2 wetting ridge dynamics (shown in the bottom left image in Fig. 8). When a slip event occurs, the contact line moves to its new position, re-pins, and forms a new wetting ridge. As the new wetting ridge grows (shown by the green star and arrow) and substrate material is transferred from the old ridge, whose height decreases (shown by the red dot and arrow). The old wetting ridge (denoted by the black dashed line) cannot fully recover its original shape due to the plastic deformation, leading to it having a relatively smooth outer slope.

Stiff substrates tend to deform elastically, and, unlike the very soft substrates, are not viscoelastic enough to trigger the horizontal motion of the wetting ridge in a viscous-flow way. This means that the wetting ridge can only grow in the vertical direction, but not move in the horizontal direction. Once a drop depins the old wetting ridge fully recovers (shown by the red circle and arrow) and a new ridge forms at the new location of the drop, as also shown in Fig. 8. For these substrates, no trace of the old wetting ridge remains outside the perimeter of the drop, as shown in the bottom right image in Fig. 8.

Let us now focus on the trigger for the transition from Regime 1 to Regime 2 in the wetting ridge dynamics.

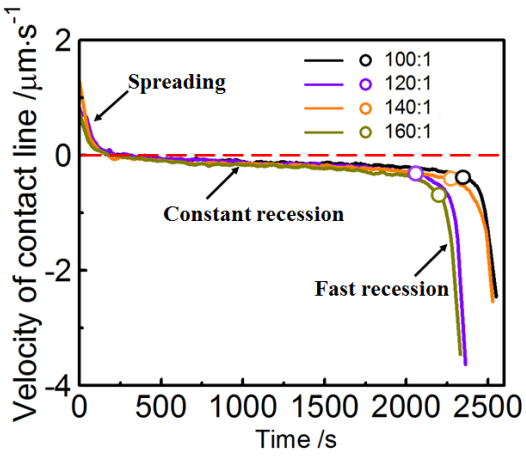

Figure 9. Evolution of the velocity of contact line of nano-suspension drops on the four softest substrates with time. Open circles indicate the transition from Regime 1 to Regime 2. The horizontal red dashed line separates the initial spreading and the subsequent receding of the contact line.

Fig. 9 shows the evolution of the velocity of the contact line for the four softest substrates (100:1–160:1) with time. Initially, the drops spread (*i.e.* have positive velocity) in each case. Then, the drops begin to slowly recede at nearly constant velocity in Regime 1 until they rapidly accelerate near the end of the evaporation at approximately 2150 s or later. This rapid acceleration coincides with the transition from Regime 1 to Regime 2, which is indicated by the open circles in Fig. 9. Hence, we can safely assert at this point that the transition to Regime 2 is dependent on the contact line velocity being faster than the viscous flow of the substrate.

The above discussion makes clear that the dynamics of a wetting ridge not only affect the final substrate deformation, but also the contact line behaviour and the evaporation kinetics of the evaporating drop. In particular, we found that, depending on the receding velocity of contact line,

two different regimes dominate in succession on very soft substrates. Moreover, we elucidated the dual roles of the wetting ridge on the contact line behaviour. On one hand, the vertical displacement of the wetting ridge can strengthen the pinning of the contact line. The higher the ridge is, the harder the contact line pins. This effect is independent of how viscoelastic the substrates are. On the other hand, the horizontal motion of the wetting ridge can induce the contact line to recede as long as the substrate is soft enough. As a result of these effects in combination, the CCR mode is extended on stiff and soft substrates, while a mixed mode accounts for most of the lifetime of the drop on very soft substrates.

Deposition patterns of nanoparticles. Fig. 10 shows the deposition patterns left behind after the complete evaporation of nano-suspension drops on each of the three different types of substrates. It is immediately apparent from the images shown in Fig. 10 that each type of surface results in a different kind of deposition pattern. On stiff substrates, particle deposits resemble a coffee ring with cracks and deposition tails. The radially- and circumferentially-oriented cracks are induced by a buckling instability, and are a common occurrence in the drying of colloidal drops on rigid substrates[40-42]. The deposition tails are located between the initial position of the contact line and that in the second CCR stage, indicating their formation occurs during the recession of the contact line (during either a CCA or a mixed mode). When the drop depins, the contact line is likely to remain pinned locally due to one or more randomly located surface defects, causing the depositing particles to form deposition tails[11]. The rest of contact line, meanwhile, recedes uniformly leading to an otherwise circular deposit. The diameters of the deposition rings coincide with the contact diameters in the second CCR mode, indicating that the nanoparticles are mainly deposited in this stage. On soft substrates, uniform rings with a diameter comparable to maximum contact diameter are formed. In contrast, on very soft

substrates, finger-like structures are formed on the crater-like deformed surfaces (see the above discussion about wetting ridge dynamics). The tips of the deposits lie at the rim of the wetting ridge which, as discussed earlier, occurs within both the initial and maximum contact diameters.

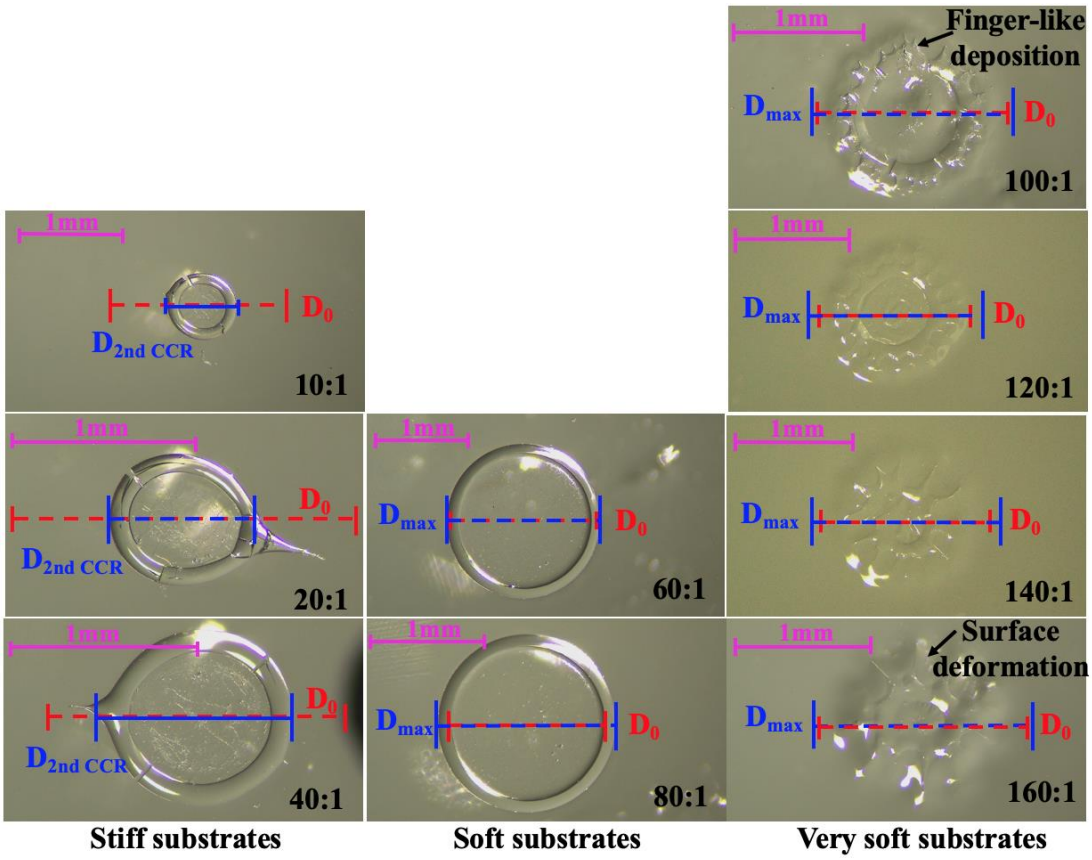

Figure 10. Deposition patterns left behind after the complete evaporation of nano-suspension drops on different viscoelastic substrates. The red dashed lines indicate the initial contact diameter, the blue solid lines indicate the contact diameter in the second CCR mode on the stiff substrates, and the blue dashed lines indicate the maximum contact diameter after initial spreading on the soft and the very soft substrates.

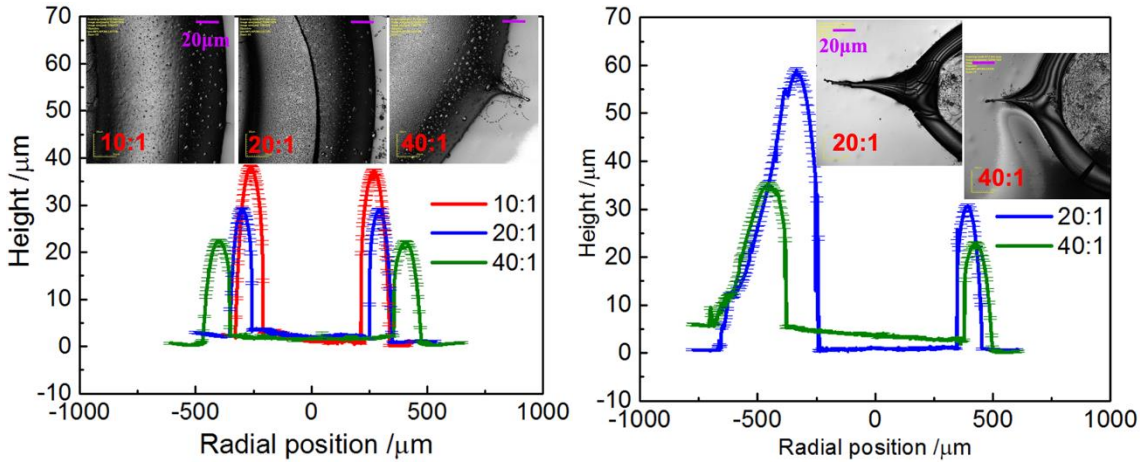

Figure 11. Cross-sectional height profiles of the deposition patterns on stiff substrates without (left-hand image) and with (right-hand image) large deposition tails. The insets show details of the local morphologies of the deposits. The magenta scale bars in the optical images are 20 μm.

Fig. 11 shows the cross-sectional height profiles of the deposition patterns on stiff substrates both with and without deposition tails, as well as details of the local morphologies of the deposits. The cross-sectional profiles of the ring deposits shown in the left-hand image in Fig. 11 are symmetrical arches with round peaks, while the symmetry of those is broken by the presence of the deposition tails described previously, shown in the right-hand image in Fig. 11.

Fig. 12 shows that the deposition patterns on soft substrates have a slightly different shape to those on stiff substrates. Specifically, the uniform ring deposits shown in Fig. 12 are thinner than those shown in Fig. 11, and their cross-sectional profiles resemble a pair of sharp ox-horns with a bent cusp leading toward the centre of the drop, similar to those described previously by Park *et al.*[21].

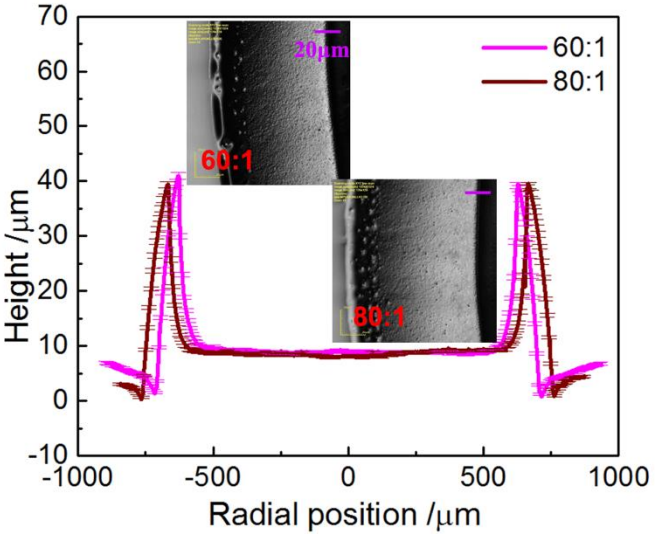

Figure 12. Cross-sectional height profiles of the deposition patterns on soft substrates. The insets show details of the local morphologies of the deposits. The magenta scale bars in the optical images are 20 μm.

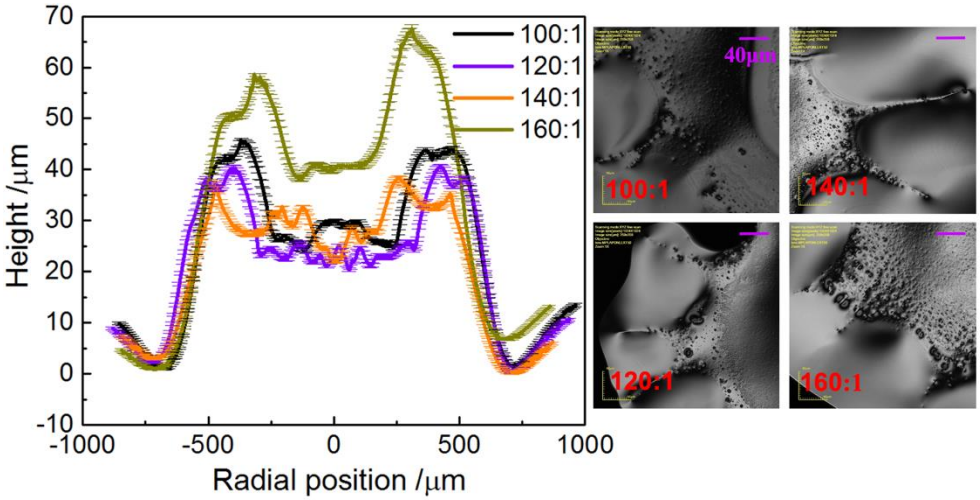

Figure 13. Cross-sectional height profiles of the deposition patterns on very soft substrates. The insets show details of the local morphologies of the deposits. The magenta scale bars in the optical images are 40 μm.

Fig. 13 shows the deposition patterns on very soft substrates. The microscope images shown in the insets reveal that the substrate has a wavy-like deformation whose highest points are covered

with the fingertips of a finger-like pattern of particles. Previous studies[18, 43-44] linked such deposition patterns to the instability of the complicated flow in the zone near the contact line, which can, in general, be due not only to the interaction of the particles, the liquid and the substrate, but also to various other physical effects, such as capillary flow, Marangoni flow and interfacial instabilities. We assume that Marangoni flow is negligible in the present experiments due to the slow evaporation of the drops[45], and thus that capillary flow is dominant[10]. Based on this hypothesis, we infer that the finger-like patterns originate from the highly viscous behaviour of the substrates, which probably behave like highly viscous layers that disturb the capillary flow. Additionally, the higher local viscosity results in stronger pinning of the contact line at the fingertips[46] and weaker pinning in between them.

By comparing the different cross-sectional profiles of the deposition patterns, we find that the height at the centre of these deposits increases with the substrate viscoelasticity: less than 5 μm on stiff substrates, about 10 μm on soft ones, and about 20–40 μm on very soft ones. This result indicates that increasing softness of the substrate reduces the coffee-ring effect, due to the fact that the deposit profiles in the left-hand image in Fig. 13 are combined profiles of the particle deposits and the deformation of the underlying substrate. Furthermore, large particle clusters can be discerned at the edges of the deposits, whereas the particles are homogenously distributed in their interiors.

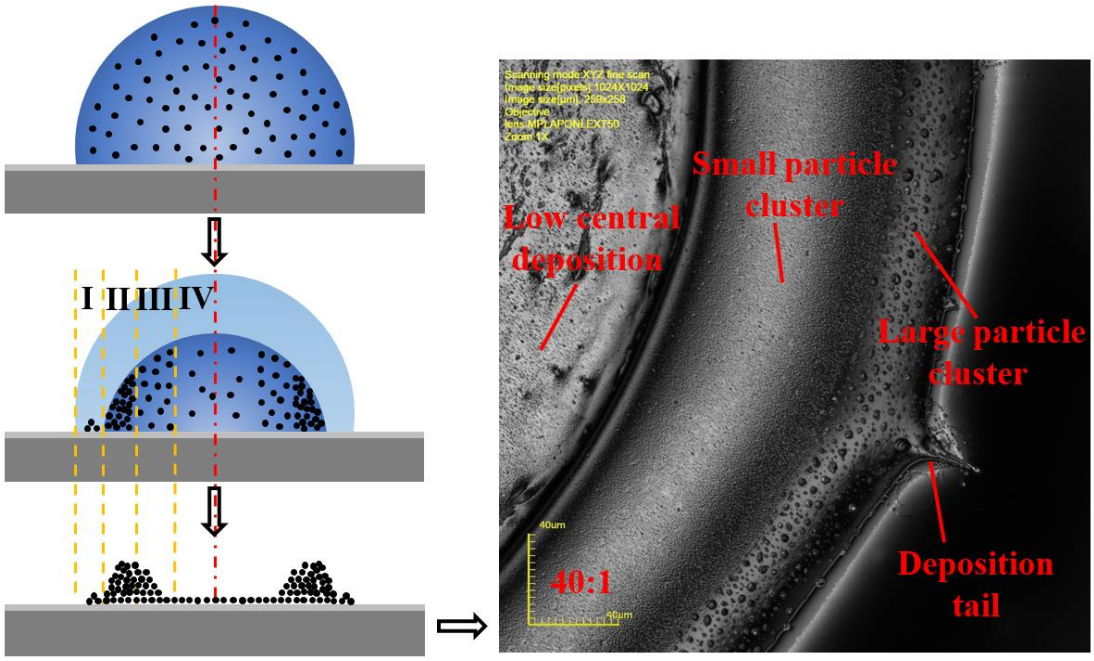

Figure 14. Schematic illustration of the process by which particles are deposited during the evaporation of nano-suspension drops, where I, II, III and IV denote the random weak pinning region, the particle aggregation region, the even distribution region, and the low particle concentration region, respectively, and an example of a deposition pattern which exhibits four different kinds of deposit in the four different regions.

Fig. 14 schematically illustrates the process by which particles are deposited during the evaporation of nano-suspension drops. The top left image shows the initial drop containing homogenously distributed particles. As the evaporation proceeds, the contact line eventually depins, but is likely to leave some particles behind at one or more randomly located substrate defects, for example, the deposition tails formed on stiff substrates described previously. This mechanism responsible for region I of the deposit shown in Fig. 14, the random weak pinning region. The second mechanism by which capillary flow transports nanoparticles to the contact line is by the replenishment of liquid due to the enhanced local evaporation during a CCR or a pseudo-CCR mode. Particles deposited in this manner easily aggregate into large particle

clusters. This mechanism is responsible for region II of the deposit, the particle aggregation region. Due to weaker confinement effects at the wedge, the region of the deposit adjacent to region II, contains relatively dilute particles compared to region II. Hence, these particles are evenly distributed either singly or in small clusters, corresponding to region III, the even distribution region. Far away from the contact line in the bulk of the drop, the wedge constraint disappears which, combined with the majority of the particles being carried to the periphery by the capillary flow, leads to a sparse distribution of particles in region IV, the low particle concentration region. After the complete evaporation, these particles form a thin deposition layer in the central area of the drop.

An example of the deposition pattern described above is shown in the right-hand image in Fig. 14, which clearly exhibits four different kinds of deposit in the four regions described above, namely (working from the exterior to the interior of the deposit): deposition tails in region I, large particle clusters in region II, small particle clusters in region III, and a thin deposition layer in region IV.

CONCLUSIONS

In the present work we studied the evaporation of sessile water and nano-suspension drops on viscoelastic substrates of a wide range of softness, including both surface deformation and particle deposition. We find that both the vertical and horizontal motions of the wetting ridge influence the evaporation kinetics. The vertical growth of the wetting ridge creates a pinning defect and results in a CCR mode, whereas the horizontal motion of the ridge depends on the softness of the substrates. In particular, the viscous-flow regime which occurs on very soft substrates allows the contact line to drag the wetting ridge with it, resulting in a mixed mode of evaporation. To the best of the authors' knowledge, this is the first study to describe this

behaviour. After complete evaporation, nanoparticles form a variety of different deposition patterns, namely coffee rings with cracks and deposition tails, uniform rings with sharp ox-horn profiles, and finger-like deposits, on stiff, soft and very soft surfaces, respectively, due to the different evaporation kinetics and the capillary flow within the evaporating drops.

The wide range of substrate viscoelasticities investigated here not only gives us an overall view of drop evaporation kinetics and particles deposition patterns, especially on very soft substrates, but also deepens our understanding of the interaction between the dynamics of the wetting ridge and the motion of the contact line. In addition, this research may shed new light on the mechanisms of drop evaporation on rigid and liquid-impregnated surfaces, which may exhibit similar behaviour. Since the substrate softness influences the nature of the deposits, it also provides us with a potential toolkit with which to control deposition patterns in a wide range of industrial applications.

AUTHOR INFORMATION

* Email of corresponding author: ksefiane@ed.ac.uk

ACKNOWLEDGEMENTS

This research was sponsored by ThermaSMART, and international and intersectoral network of organisations working on a joint research programme in the area of phase-change cooling of high-power electronic devices, funded from the European Research Council under the European Union's Horizon 2020 Research and Innovation Programme (grant agreement no. 778104). The first author (YC) is supported by a China Scholarships Council (CSC) Scholarship.

REFERENCES

1. Roman, B.; Bico, J., Elasto-capillarity: deforming an elastic structure with a liquid droplet. *Journal of Physics. Condensed Matter* **2010,** *22* (49), 493101.

2. Huh, D.; Matthews, B. D.; Mammoto, A.; Montoya-Zavala, M.; Hsin, H. Y.; Ingber, D. E., Reconstituting organ-level lung functions on a chip. *Science* **2010,** *328* (5986), 1662-1668.

3. Lopes, M. C.; Bonaccurso, E., Evaporation control of sessile water drops by soft viscoelastic surfaces. *Soft Matter* **2012,** *8* (30), 7875-7881.

4. Py, C.; Reverdy, P.; Doppler, L.; Bico, J.; Roman, B.; Baroud, C. N., Capillary origami: spontaneous wrapping of a droplet with an elastic sheet. *Physical Review Letters* **2007,** *98* (15), 156103.

5. Picknett, R. G.; Bexon, R., The evaporation of sessile or pendant drops in still air. *Journal of Colloid and Interface Science* **1977,** *61* (2), 336-350.

6. Orejon, D.; Sefiane, K.; Shanahan, M. E., Stick-slip of evaporating droplets: substrate hydrophobicity and nanoparticle concentration. *Langmuir* **2011,** *27* (21), 12834-12843.

7. Stauber, J. M.; Wilson, S. K.; Duffy, B. R.; Sefiane, K., On the lifetimes of evaporating droplets. *Journal of Fluid Mechanics* **2014,** *744*, R2.

8. Schofield, F. G. H.; Wilson, S. K.; Pritchard, D.; Sefiane, K., The lifetimes of evaporating sessile droplets are significantly extended by strong thermal effects. *Journal of Fluid Mechanics* **2018,** *851*, 231-244.

9. Stauber, J. M.; Wilson, S. K.; Duffy, B. R.; Sefiane, K., On the lifetimes of evaporating droplets with related initial and receding contact angles. *Physics of Fluids* **2015,** *27* (12), 122101.

10. Deegan, R. D.; Bakajin, O.; Dupont, T. F.; Huber, G.; Nagel, S. R.; Witten, T. A., Capillary flow as the cause of ring stains from dried liquid drops. *Nature* **1997,** *389* (6653), 827-829.

11. Askounis, A.; Orejon, D.; Koutsos, V.; Sefiane, K.; Shanahan, M. E. R., Nanoparticle deposits near the contact line of pinned volatile droplets: size and shape revealed by atomic force microscopy. *Soft Matter* **2011,** *7* (9), 4152-4155.

12. Parsa, M.; Harmand, S.; Sefiane, K.; Bigerelle, M.; Deltombe, R., Effect of substrate temperature on pattern formation of nanoparticles from volatile drops. *Langmuir* **2015,** *31* (11), 3354-3367.

13. Askounis, A.; Sefiane, K.; Koutsos, V.; Shanahan, M. E., Effect of particle geometry on triple line motion of nano-fluid drops and deposit nano-structuring. *Advances in Colloid and Interface Science* **2015,** *222*, 44-57.

14. Uno, K.; Hayashi, K.; Hayashi, T.; Ito, K.; Kitano, H., Particle adsorption in evaporating droplets of polymer latex dispersions on hydrophilic and hydrophobic surfaces. *Colloid and Polymer Science* **1998,** *276* (9), 810-815.

15. Hu, H.; Larson, R. G., Marangoni effect reverses coffee-ring depositions. *The Journal of Physical Chemistry B* **2006,** *110* (14), 7090-7094.

16. Jing, G.; Ma, J., Formation of circular crack pattern in deposition self-assembled by drying nanoparticle suspension. *The Journal of Physical Chemistry B* **2012,** *116* (21), 6225-6231.

17. Brutin, D.; Sobac, B.; Loquet, B.; Sampol, J., Pattern formation in drying drops of blood. *Journal of Fluid Mechanics* **2011,** *667*, 85-95.

18. Gonuguntla, M.; Sharma, A., Polymer patterns in evaporating droplets on dissolving substrates. *Langmuir* **2004,** *20* (8), 3456-3463.

19. Style, R. W.; Dufresne, E. R., Static wetting on deformable substrates, from liquids to soft solids. *Soft Matter* **2012,** *8* (27), 7177-7184.

20. Style, R. W.; Boltyanskiy, R.; Che, Y.; Wettlaufer, J. S.; Wilen, L. A.; Dufresne, E. R., Universal deformation of soft substrates near a contact line and the direct measurement of solid surface stresses. *Physical Review Letters* **2013,** *110* (6), 066103.

21. Park, S. J.; Weon, B. M.; Lee, J. S.; Lee, J.; Kim, J.; Je, J. H., Visualization of asymmetric wetting ridges on soft solids with X-ray microscopy. *Nature Communications* **2014,** *5*, 4369.

22. Park, S. J.; Bostwick, J. B.; De Andrade, V.; Je, J. H., Self-spreading of the wetting ridge during stick-slip on a viscoelastic surface. *Soft Matter* **2017,** *13* (44), 8331-8336.

23. Kajiya, T.; Daerr, A.; Narita, T.; Royon, L.; Lequeux, F.; Limat, L., Advancing liquid contact line on visco-elastic gel substrates: stick-slip vs. continuous motions. *Soft Matter* **2013,** *9* (2), 454-461.

24. Rusanov, A. I., Theory of wetting of elastically deformed bodies. 1. Deformation with a finite contact-angle. *Colloid Journal of the USSR* **1975,** *37* (4), 614-622.

25. Pericet-Camara, R.; Auernhammer, G. K.; Koynov, K.; Lorenzoni, S.; Raiteri, R.; Bonaccurso, E., Solid-supported thin elastomer films deformed by microdrops. *Soft Matter* **2009,** *5* (19), 3611-3617.

26. Yu, Y. S.; Zhao, Y. P., Elastic deformation of soft membrane with finite thickness induced by a sessile liquid droplet. *Journal of Colloid and Interface Science* **2009,** *339* (2), 489-944.

27. Pu, G.; Severtson, S. J., Water evaporation on highly viscoelastic polymer surfaces. *Langmuir* **2012,** *28* (26), 10007-10014.

28. Yu, Y.-S.; Wang, Z.-Q.; Zhao, Y.-P., Experimental study of evaporation of sessile water droplet on PDMS surfaces. *Acta Mechanica Sinica* **2013,** *29* (6), 799-805.

29. Lopes, M. C. Bonaccurso, E., Influence of substrate elasticity on particle deposition patterns from evaporating water–silica suspension droplets. *Soft Matter* **2013,** *9* (33), 7942-7950.

30. Deegan, R. D., Pattern formation in drying drops. *Physical Review E* **2000,** *61* (1), 475-485.

31. Chen, L.; Auernhammer, G. K.; Bonaccurso, E., Short time wetting dynamics on soft surfaces. *Soft Matter* **2011,** *7* (19), 9084-9089.

32. Shanahan, M. E. R., The spreading dynamics of a liquid drop on a viscoelastic solid. *Journal of Physics D: Applied Physics* **1988,** *21* (6), 981-985.

33. Carré, A.; Shanahan, M. E. R., Effect of cross-linking on the dewetting of an elastomeric surface. *Journal of Colloid and Interface Science* **1997,** *191* (1), 141-145.

34. Kuchin, I.; Starov, V., Hysteresis of contact angle of sessile droplets on smooth homogeneous solid substrates via disjoining/conjoining pressure. *Langmuir* **2015,** *31* (19), 5345-5352.

35. Lopes, M. C., Chapter 12 - Soft Substrates. In *Droplet Wetting and Evaporation*, Brutin, D., Ed. Academic Press: Oxford, 2015; pp 157-171.

36. Shanahan, M. E. R.; Carré, A., Viscoelastic dissipation in wetting and adhesion phenomena. *Langmuir* **1995,** *11* (4), 1396-1402.

37. Smith, J. D.; Dhiman, R.; Anand, S.; Reza-Garduno, E.; Cohen, R. E.; McKinley, G. H.; Varanasi, K. K., Droplet mobility on lubricant-impregnated surfaces. *Soft Matter* **2013,** *9* (6), 1772-1780.

38. Khalil, K. S.; Mahmoudi, S. R.; Abu-dheir, N.; Varanasi, K. K., Active surfaces: ferrofluid-impregnated surfaces for active manipulation of droplets. *Applied Physics Letters* **2014,** *105* (4), 041604.

39. Pu, G.; Severtson, S. J., Characterization of dynamic stick-and-break wetting behavior for various liquids on the surface of a highly viscoelastic polymer. *Langmuir* **2008,** *24* (9), 4685-4692

40. Brutin, D.; Sobac, B.; Nicloux, C., Influence of substrate nature on the evaporation of a sessile drop of blood. *Journal of Heat Transfer* **2012,** *134* (6), 061101.

41. Pauchard, L.; Parisse, F.; Allain, C., Influence of salt content on crack patterns formed through colloidal suspension desiccation. *Physical Review E* **1999,** *59* (3), 3737-3740.

42. Askounis, A.; Sefiane, K.; Koutsos, V.; Shanahan, M. E. R., The effect of evaporation kinetics on nanoparticle structuring within contact line deposits of volatile drops. *Colloids and Surfaces A: Physicochemical and Engineering Aspects* **2014,** *441*, 855-866.

43. Klentzman, J.; Ajaev, V. S., The effect of evaporation on fingering instabilities. *Physics of Fluids* **2009**, 21 (12), 122101.

44. Yang, X.; Li, C. Y.; Sun, Y., From multi-ring to spider web and radial spoke: competition between the receding contact line and particle deposition in a drying colloidal drop. *Soft Matter* **2014**, 10 (25), 4458-63.

45. Larson, R. G., Transport and deposition patterns in drying sessile droplets. *AIChE Journal* **2014,** *60* (5), 1538-1571.

46. Askounis, A.; Sefiane, K.; Koutsos, V.; Shanahan, M. E., Structural transitions in a ring stain created at the contact line of evaporating nanosuspension sessile drops. *Physical Review E* **2013,** *87* (1), 012301.

TABLE OF CONTENTS GRAPHIC